Georadar data processing and imaging: paleoseismicity in the Piano di Castelluccio Basin, Central Italy

Robert J. Ferguson, Maurizio Ercoli, and Alessandro Frigeri

ABSTRACT

Three georadar lines are presented in a comparison of conventional georadar processing flows and flows based on the `gabordecon` algorithm from the CREWES toolbox. The imaging goal is to map near-surface sediments above a Quaternary fault in the Piano di Castelluccio Basin in central Italy. There is a history of earthquake risk in this region and the georadar data were acquired for infrastructure planning as part of Probabilistic Seismic Hazard Assessment (PSHA) in Italy. The georadar data are used to tie reflection seismological fault images to the surface. We find that the `gabordecon`-based flow is significantly better than the conventional flow and this is likely due to Q compensation characteristics that are intrinsic to `gabordecon`.

INTRODUCTION

A strong 1703 earthquake is thought to be related to the Norcia fault system in Central Italy so there is significant interest in fault imaging for this region (Galadini and Galli, 2009). To the East of the Norcia system is a parallel set of faults called the Mount Verrore fault (Galadini and Galli, 2009). This fault is considered to be seismically stable because no known earthquake has been attributed to it (Galadini and Galli, 2009). The only evidence of the existence of this fault comes from geomorphological studies and trenching(Galadini and Galli, 2009).

The potential exists for seismic data acquisition in this region, and the georadar acquisition that is under consideration here was acquired to identify and tie fault exposures to the seismic data. A 300 MHz centre frequency antenna system was deployed on a 20 m $\times$ 20 m grid with sub-decimetre station intervals (Ercoli et al., 2012). There are 201 profiles of 401 georadargams each in this dataset (Ercoli et al., 2012).

In this report, we investigate the utility of a pre-processing algorithm that is usually applied to seismic data, and we compare this result to pre-processing using a more conventional georadar processing flow (Ercoli et al., 2012, for example). Gabor deconvolution (Margrave et al., 2011) (`gabordecon` in the CREWES toolbox) is the major difference between the seismic-based flow and the conventional flow, and we ignore the application of a *de-wow* filter. We find that our seismic-based flow provides as substantially better image than the conventional flow. We find significant improvement in all aspects of signal quality including broader bandwidth, improved near-surface (< 1 m) imaging, and we find that signal length limits our ability to draw reflection energy from much deeper in the section than the conventional flow.

GEOLOGY AND PALEOSEISMICITY

The goal of the georadar survey is to image the near-surface sediments above a Quaternary fault in the Piano di Castelluccio Basin in central Italy for infrastructure planning

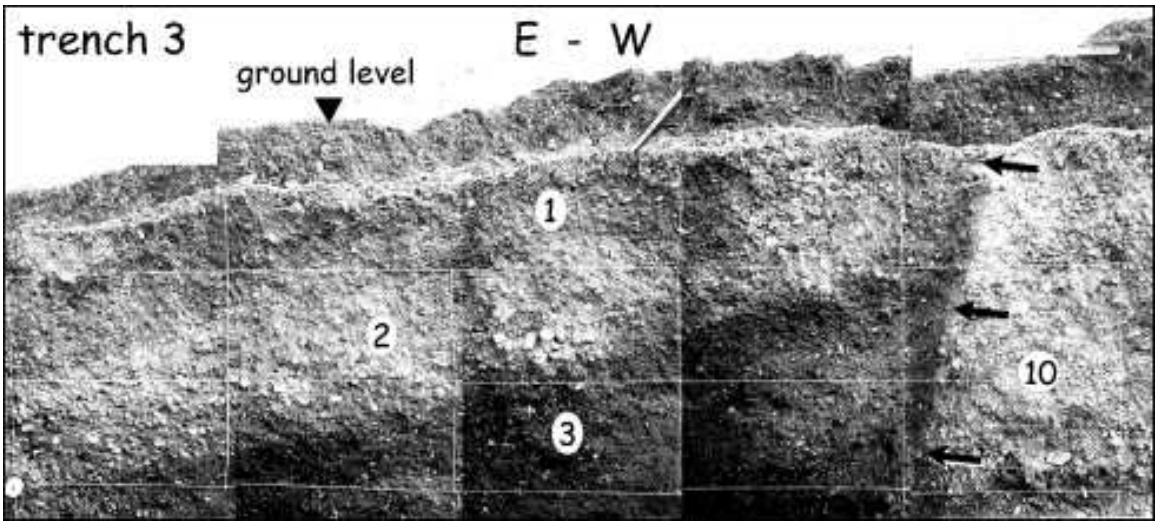

FIG. 1. Outcrop indicating faulting through the near surface (black arrows). Image courtesy of Galli et al. (2005).

(Ercoli et al., 2012) and as part of Probabilistic Seismic Hazard Assessment (PSHA) in Italy to tie reflection seismological fault images (Galadini and Galli, 2009; Boncio et al., 2004) to the surface (Figure 1). Two sand units above a gravel unit in the upper few meters - the two sands are distinguished by the higher organic content of the lower of the two sands (Galadini and Galli, 2009; Ercoli et al., 2012). As an example of what the image target looks like, an annotated photograph of an outcropping fault is shown in Figure 1.

GEORADAR ACQUISITION

Georadar acquisition design optimizes the image of a small area around a known fault. The georadar grid is intended as a proof that georadar can be used to tie the very near surface (<10's m) to the deeper section (Ercoli et al., 2012). Specifically, sub-decimetre trace intervals are used so that migration of the georadar 3D is possible.

The acquisition parameters are specified in Table 1. A 20 m $\times$ 20 m grid was acquired with an inline spacing of 5 cm and a crossline spacing of 10 cm for a 401 $\times$ 201 trace grid and 80,601 total traces. A 16 bit Zond recorder with 300 MHz centre frequency antennas were deployed, and each trace represents the vertical stack of 8 traces. The trace length is 512 samples where the first 11 samples are not gained to reduce the effect of the direct arrival, and the time interval between samples $(\Delta t) = 0.2\,\eta$s.

CONVENTIONAL PROCESSING

The goal of conventional georadar processing is to cope with the natural bias in the recorded radar signal (this is referred to as "wow" by the georadar community), and to shift the data first-arrival to zero-time (Reflexw, 2012). The specifics of the baseline processing flow is given in Table 2. A trace average filter is applied to reduce noise, and elevation statics are applied though there is not significant topography in the area.

Acquisition design	Parameters
Survey	GIS mapping GPS positioning
Grid	20 $\times$ 20 m
Recording instrument	Zond (16 bit) `radsys.lv`
Centre frequency	300 MHz
Vertical stack	8 traces
Number of inline traces	401
Inline interval (Δx)	5 cm
Number of crossline traces	201
Crossline interval (Δy)	10 cm
Trace length	100 ηs
Time interval (Δt)	0.2 ηs

Table 1. Castelluccio di Norcia 3D georadar acquisition parameters (Ercoli et al., 2012).

Process	Parameters
Trace edit	
De-wow (low-cut filter)	3.3 ηs (pulse width)
First-break flattening	
Gain	Exponential
Band-pass filter	65-90 450-550 MHz
Top mute	0-16 ηs
2D average filter	4 traces $\times$ 8 samples
Elevation statics	

Table 2. Baseline processing parameters.(Ercoli et al., 2012).

SEISMIC-BASED PROCESSING

Rather than apply a de-wow filter as is done in the conventional flow, we recognize that the procedure is effectively a high-pass filter. We find that Gabor decon (Margrave et al., 2011) excludes the bias because our decon design frequency range (80 - 500 MHz) excludes the bias range. Our seismic-based processing is given in detail in Table 3, and in particular we follow these rules of thumb for Gabor decon: 1) use hyperbolic smoothing. 2) The frequency smoother (`fsmo` in `gabordecon`) should be close to the centre frequency of the data. 3) The Gaussian width (`twin`) should be about the width of the wavelet. 4) The temporal smoother (`tsmo`) should be about 5 $\times$ the Gaussian width.

Process	Parameters
Top mute	0-16 ns
Segy read	`altreadsegy` (from the CREWES processing toolbox)
Gabor deconvolution	`gabordecon` (from the CREWES processing toolbox). `twin`=20/f_{Nyq}, `tinc`=3/2/f_{Nyq}, `tsmo`=80/f_{Nyq}, `fsmo`=440 MHz, Hyperbolic smoothing, `stab`=0, minimum phase, Synthesis window is unity, `gdb`=60.
Bandpass filter	80-500 MHz

Table 3. Gabor processing flow parameters.

DATA EXAMPLES

Three lines from the 3D volume are extracted and processed as a demonstration. The raw data from these lines are shown in Figures 2 through 4 along with the conventional processing and our seismic-based processing. In Figure 2(a), the raw data is dominated by strong amplitudes associated with the first arrivals plus a strong monochromatic wave that is observed with low ground-coupling and when we encounter conductive soil. Conventional processing (Figure 2(b)) reduces the reverberation and it does bring out many reflection events with a dim region between trace numbers 250 and 300. Our processing flow (Figure 2(c)) does a much better job or trace-to-trace balancing, reflection events are much sharper, and significant detail is present with very high fidelity in particular in the upper 10 ns of the section. The dim region that is evident on Figure 2(b) is very nicely resolved with our flow. Note that, for each of lines 40, 100, and 160 (Figures 2(c), 3(c), and 4(c)), coherent reflection energy persists through to the end of the recordings and that, clearly, reflection energy is obtainable from much deeper in the section.

Data from line 100 are shown in Figures 3(a) through 3(c). The data gap that is evident on the conventional image (Figure 3(b)) has been filled in by our flow. This gap is due to a mute of the raw data applied during previous processing. In Figure 3(c) we see that this gap is filled in by our processing flow. Though the rest of the section is improved in a way that is consistent with the improvements seen in line 40, erroneous reflection events are generated by Gabor decon within what we know is a mute zone. Legitimate no-data zones (for example excavation of a trench that obliterates soil boundaries) will also be infilled in this way. A remedy for this *infilling* effect is currently not apparent.

Data for line 160 are shown in Figures 4(a) through 4(c). Dimming of reflections on the left hand side of the conventional section (Figure 4(b)) is very nicely remedied by our flow (Figure 4(c)), and significant detail is brought out in every region of the section. Again, reflection data beyond the end of the section must surely be available.

Spectra for lines 40, 100, and 160 are given in Figures 5 through 7. The raw spectra (Figures 5(a), 6(a), and 7(a)) are all dominated by sub-300 MHz (the centre frequency of the antenna) energy. Conventional processing (Figure 5(b), 6(b), and 7(b)) does de-wow (low-cut filter) the data, but not much detail is extracted above 300 MHz and the spatial balance of the spectrum is uneven. Our flow is likely extracting signal beyond 400 MHz (Figures 5(c), 6(c), and 7(c)), and the spatial balance is much better. The exception, as indicated earlier, is with line 100 where what is probably a trench is now filled in with erroneous reflection data. The spectrum (Figure 6(c)) indicates that our flow has introduced a strong band of amplitude centred around 200 MHz between trace 15 and trace 130.

CONCLUSIONS

We present here a comparison of conventional georadar processing and seismic-based processing that includes Gabor deconvolution as implemented by CREWES (`gabordecon` in the CREWES toolbox). The data consist of three 2D lines extracted from a 3D georadar volume. This volume was acquired as part of a paleoseismological study in Central Italy. The goal of the study is to tie georadar images of what might be active faults in the near surface to deeper seismic images of the same faults. We find that overall, our seismic-based processing flow returns images that have much greater definition of reflection events and that trace to trace balance is excellent. One exception is in the region of what we know is a mute zone. Here, we feel that Gabor decon introduces spurious energy that is centred around 200 MHz though we are not confident yet as to the mechanism behind this nor how to eliminate it. We note that longer recording times should be considered as our flow brings out coherent reflection energy to the end of the current recording time. A longer recording time then coupled with our flow should resolve even deeper reflection events.

ACKNOWLEDGEMENTS

I wish to thank the staff and sponsors of CREWES for their support. I also thank NSERC for their support of this work through CRD grant CRDPJ 379744-08.

REFERENCES

Boncio, P., G. Lavecchia, and B. Pace, 2004, Defining a model of 3d seismogenic sources for seismic hazard assessment applications: The case of central apennines (italy): Journal of Seismology, **8**, no. 3, 407–425. (10.1023/B:JOSE.0000038449.78801.05).

Ercoli, M., C. Pauselli, C. Federico, A. Frigeri, and E. Forte, 2012, 3D GPR imaging for paleoseismology in central appennines (Italy): Ground Penetrating Radar (GPR), 2012 14th International Conference on, 937 –942.

Galadini, F., and P. Galli, 2009, Paleoseismology of silent faults in the central apennines (italy): the mt. vettore and laga mts. faults: Annals of Geophysics, **46**.

Galli, P., F. Galadini, and F. Calzoni, 2005, Surface faulting in norcia (central italy): a paleoseismological perspective: Tectonophysics, **403**, 117 – 130.

Margrave, G. F., M. P. Lamoureux, and D. C. Henley, 2011, Gabor deconvolution: Estimating reflectivity by nonstationary deconvolution of seismic data: Geophysics, **76**, W15–W30.

Reflexw, 2012, Manual of georadar processing.

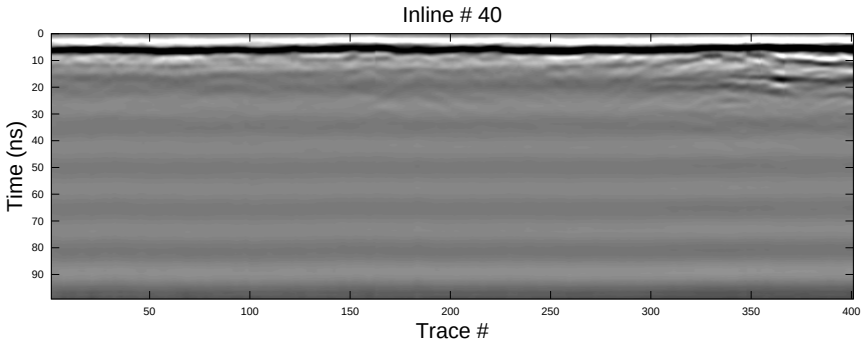

(a)

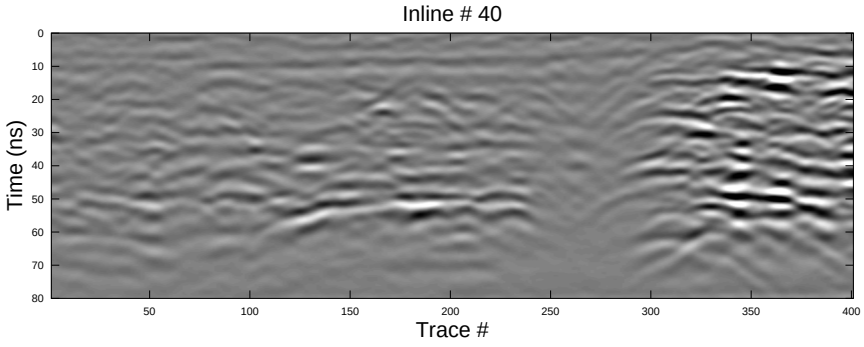

(b)

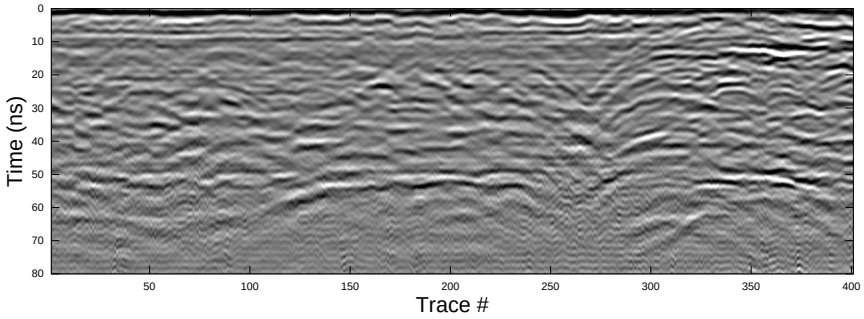

(c)

FIG. 2. Line 40: a) The raw data with a 65-90-450-550 MHz bandpass filter applied. b) Image from conventional processing. c) Image from seismic-based processing.

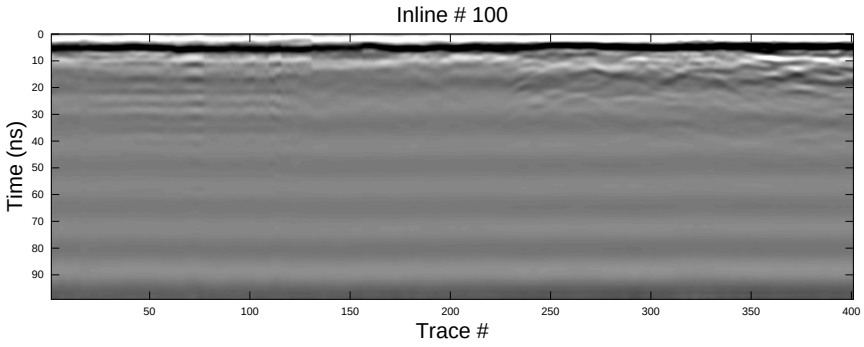

(a)

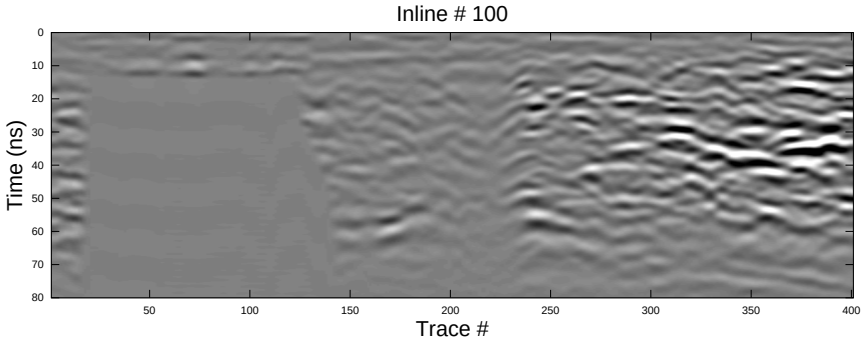

(b)

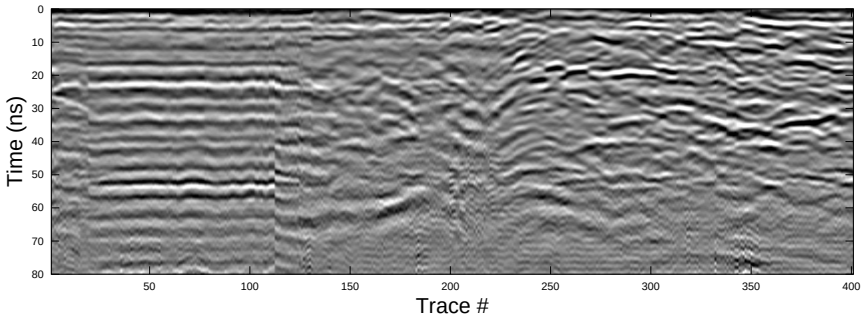

(c)

FIG. 3. Line 100: a) The raw data with a 65-90-450-550 MHz bandpass filter applied. Note the missing data area. b) Image from conventional processing. c) Image from seismic-based processing.

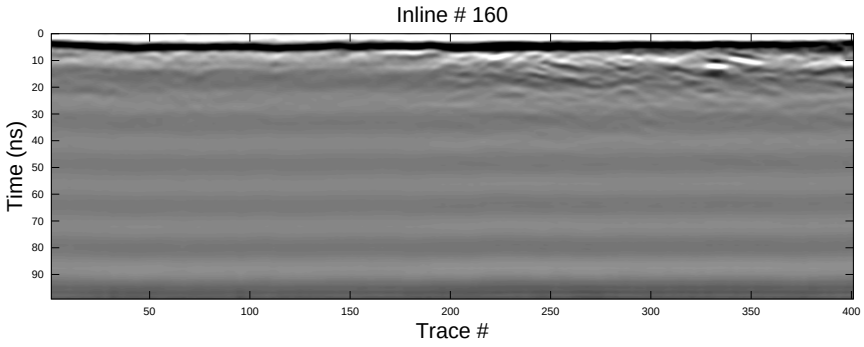

(a)

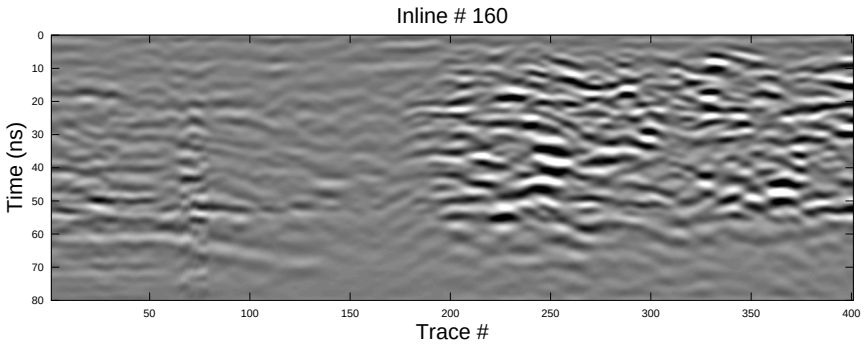

(b)

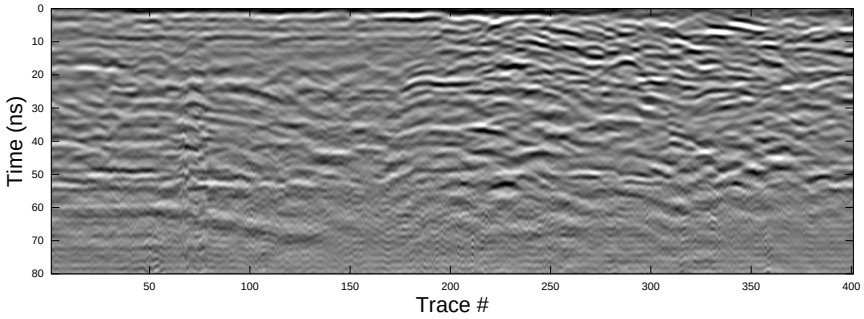

(c)

FIG. 4. Line 160: a) The raw data with a 65-90-450-550 MHz bandpass filter applied. b) Image from conventional processing. c) Image from seismic-based processing.

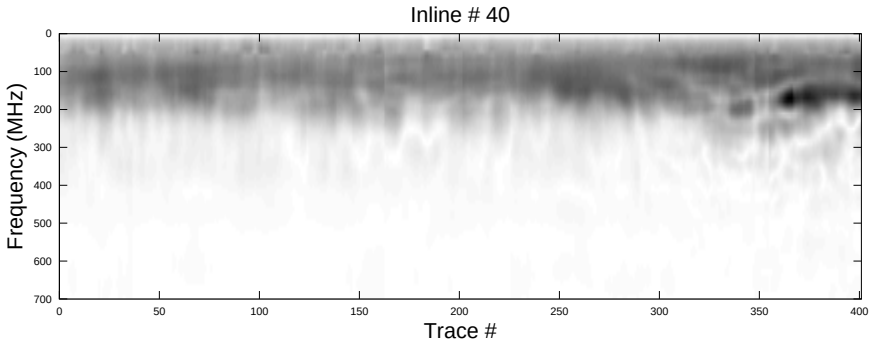

(a)

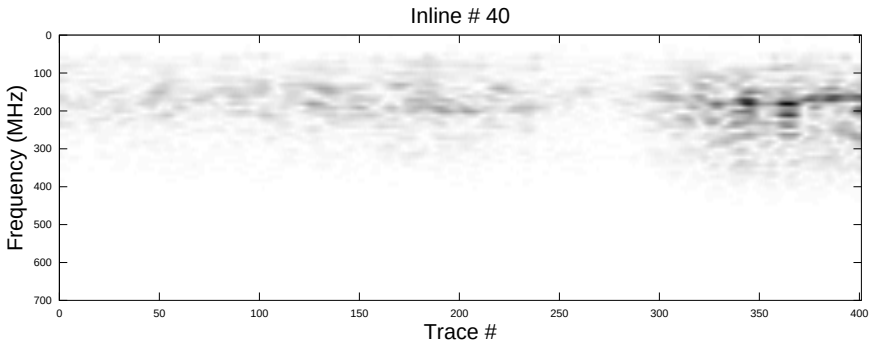

(b)

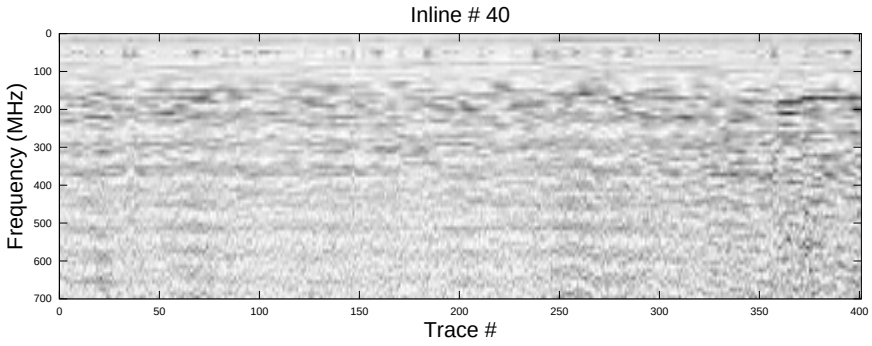

(c)

FIG. 5. Spectra for line 40: a) Raw data. b) Image from conventional processing. c) Image from seismic-based processing.

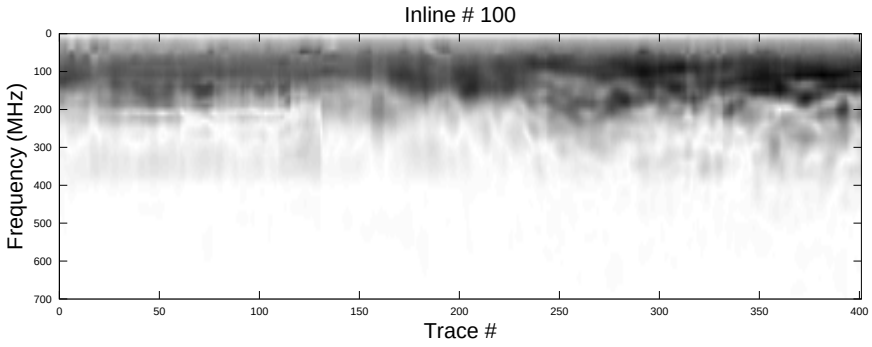

(a)

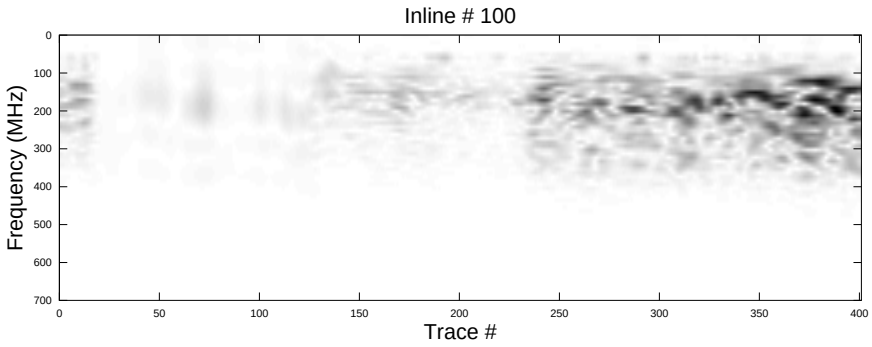

(b)

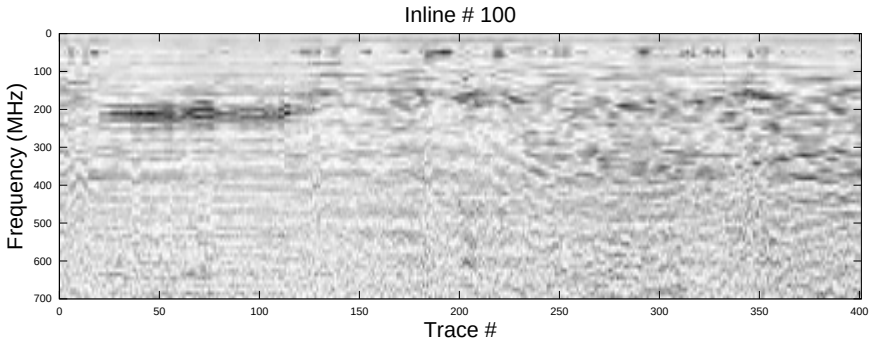

(c)

FIG. 6. Spectra for line 100: a) Raw data. b) Image from conventional processing. c) Image from seismic-based processing.

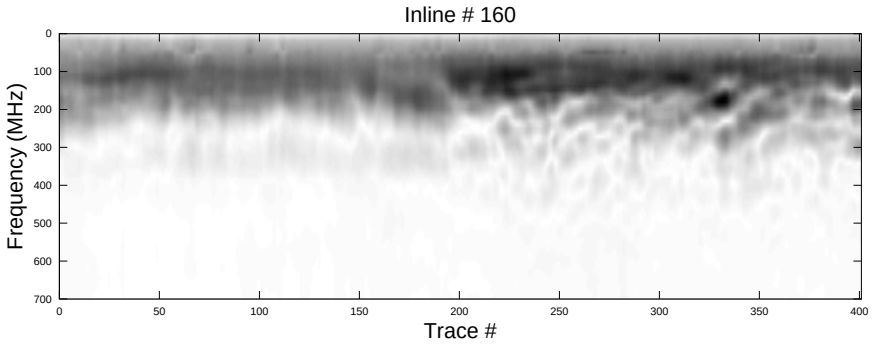

(a)

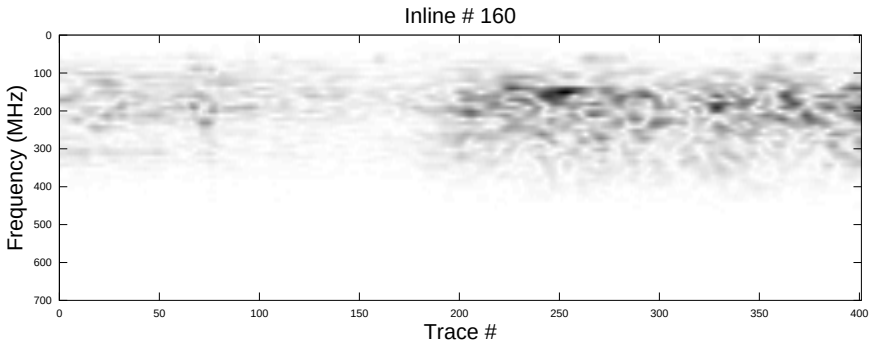

(b)

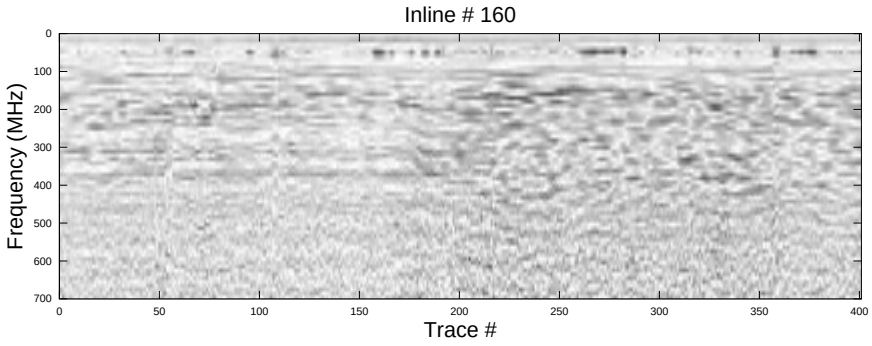

(c)

FIG. 7. Spectra for line 160: a) Raw data. b) Image from conventional processing. c) Image from seismic-based processing.